Prediction of the autogenous shrinkage and microcracking of alkali-activated slag and fly ash concrete

Li, Zhenming; Lu, Tianshi; Chen, Yun; Wu, Bei; Ye, Guang

DOI
10.1016/j.cemconcomp.2020.103913

Publication date
2021

Document Version
Final published version

Published in
Cement and Concrete Composites

Cement and Concrete Composites 117 (2021) 103913

Contents lists available at ScienceDirect

Cement and Concrete Composites

journal homepage: http://www.elsevier.com/locate/cemconcomp

Prediction of the autogenous shrinkage and microcracking of alkali-activated slag and fly ash concrete

Zhenming Li [a,1], Tianshi Lu [a,*,1], Yun Chen [a,b], Bei Wu [a], Guang Ye [a,c]

[a] Department of Materials, Mechanics, Management & Design, Faculty of Civil Engineering and Geoscience, Delft University of Technology, Delft, the Netherlands
[b] School of Materials Science and Engineering, South China University of Technology, Guangzhou, 510640, Guangdong, China
[c] Magnel Laboratory for Concrete Research, Department of Structural Engineering, Ghent University, Ghent, Belgium

ARTICLE INFO

Keywords:
Prediction
Alkali-activated slag and fly ash
Autogenous shrinkage
Creep
Aggregate
Microcracking

ABSTRACT

This study aims to predict the autogenous shrinkage of alkali-activated concrete (AAC) based on slag and fly ash. A variety of analytical and numerical models are available for the prediction of autogenous shrinkage of ordinary Portland cement (OPC) concrete, but these models are found to show dramatic discrepancies when applied for AAC due to the different behaviours of these two systems. In this study, a new numerical approach is developed to predict the autogenous shrinkage of alkali-activated slag (AAS) and alkali-activated slag-fly ash (AASF) concrete from the experimental results on corresponding paste. In this approach, the creep of AAS and AASF and the restraining effect of the aggregate are particularly considered. By this approach, a fairly good prediction is obtained. Moreover, the microcracking in paste caused by restraining aggregates is evaluated. The results indicate that AAC is subjected to high tendency of development of microcracking.

1. Introduction

In the past decade, alkali-activated materials (AAMs) are gaining increasing academic and industrial attention [1]. A major motivation of studying the performances of AAMs comes from their promising potential to replace ordinary Portland cement (OPC) in concrete. As the concern about global warming grows in recent years, people are trying to find alternative binders to OPC since the production of cement contributes considerably to the CO_2 emission worldwide [2,3]. With alkali-activation, many aluminosilicate precursors can show reactivity and binding property, thus can be used with aggregates to produce concrete, where OPC can be 100% substituted. Another benefit of using AAMs based concrete lies in the potential to repurpose industrial by-products and to reduce waste material deposition. Many industrial by-products and wastes, such as slag, fly/bottom ash, municipal solid waste incineration ash, glass powder, wastepaper sludge, etc., have been given opportunities to be reused through the technology of alkali-activation [4–7].

The two most reused raw materials to make alkali-activated concrete (AAC) are blast furnace slag from the production of steel and fly ash from the electricity plants firing coal. Alkali-activated slag (AAS) and alkali-activated slag-fly ash (AASF) can show comparable or even superior performances to those of OPC systems [8,9]. However, a wide application of alkali-activated slag and fly ash materials in engineering is still not realized yet. One of the main reasons for that is the lack of standards of AAC. To lay the basis of standardization of AAC, it is essential to undertake research and development on mechanical property, durability, volume stability, etc., of this material [4]. On the former two properties, active research has been being conducted [10,11]. For example, two Rilem Technical Committees, TC-CAM and TC-DTA, have been doing their work on durability of AAMs. Rilem TC-MPA on mechanical properties of AAC is just started. Methodologies for testing the durability and mechanical properties of AAC are being validated [12,13]. By contrast, much less research effort has been put into the volume stability, especially the autogenous shrinkage of AAC [14–16].

Autogenous shrinkage is an important property since it develops fast at early age and can induce a series of problems in aspects of aesthetics, deflection, and cracking of concrete [17,18]. The cracks, in either macro scale or micro scale, can further induce secondary problems [19], for example, interfering the serviceability and durability of concrete. Although many studies have been conducted on the magnitudes [20–23], mechanisms [24–26] and mitigating strategies [27–29] of autogenous shrinkage of AAC, the research on the prediction of autogenous shrinkage of AAC is still rare. Identifying accurate models for the

* Corresponding author.
E-mail address: lutianshi2017@gmail.com (T. Lu).
[1] The first two authors contributed to this work equally

https://doi.org/10.1016/j.cemconcomp.2020.103913
Received 11 September 2020; Received in revised form 18 November 2020; Accepted 21 December 2020
Available online 24 December 2020

prediction of autogenous shrinkage of AAC is vital not only for the establishment of relative standards on AAC but also for limiting the costs of laboratory tests [30].

The first objective of this study is to check whether the existing models to predict the autogenous shrinkage of OPC concrete can be used for AAC. For OPC concrete, various types of predicting models have been proposed. These models can be classified as analytical model [31,32], composite model (also called classic mechanical model) [33–35], finite element model [36] and lattice discrete model [37], etc. Analytical models based on phenomenological approach are handy for engineering practice and are available in standard codes, e.g. *fib* Model Code, Eurocode, ACI 209 code [38]. It is meaningful to check the accuracy of the analytical models for OPC concrete in predicting the autogenous shrinkage of AAC from the experimental parameters that are easier to obtain. With proper inputs, both finite element model and lattice discrete model can be used to predict the bulk (e.g. thermal and autogenous) deformation of the concrete [39,40]. In particular, lattic model can provide details on local strain distribution and microcracks under tensile stress [41]. However, these models normally require a relatively long time of calculation. Moreover, there is no sufficient information yet on the microstructure and micromechanical properties of AAMs to provide inputs for these models [42]. Therefore, finite element model and lattice discrete model may not be readily available to be used in shrinkage prediction of AAC. Composite models, including Pickett's model, Hobbs' model, Tazawa's model, etc., are based on classic mechanics and are able to predict the autogenous shrinkage of concrete from the autogenous shrinkage of corresponding paste. For OPC concrete, the composite models have shown satisfactory predictions [43], but whether these models are applicable in AAC remains unanswered.

According to the literature [14,24], AAC can show much more pronounced viscoelasticity than OPC concrete, while the composite models are based on elastic mechanics. Therefore, an extension of the existing composite models to take into account of the viscoelastic deformation, viz. creep of AAC might be desired. Hence, the second objective of this paper is to develop a reliable model to predict the autogenous shrinkage of AAC, possibly by extending the current composite model.

In this paper, the materials, mixtures and experimental results that are used as inputs of modelling are shown at first. Afterwards, the applicability of existing autogenous shrinkage models, i.e., analytical model based on *fib* Model Code 2010 and Pickett's model for OPC concrete are examined. Based on analysing the discrepancies between the predicted and measured autogenous shrinkage, a new numerical approach (extended Pickett's model) is developed, which shows a much better prediction by taking into account of the creep of AAC. In the last part of this study, the extended Pickett's model is used to calculate the tangential tensile stress in the paste surrounding aggregates, based on which the tendency of microcracking induced by the restraining effect of aggregate in AAC is evaluated.

2. Materials and mixtures

2.1. Materials

Slag and fly ash were used as precursors to synthesize AAS and AASF paste and concrete. The chemical compositions and physical properties of slag and fly ash are shown in Table 1.

The alkaline activator was prepared by mixing deionized water, NaOH pellets and Na_2SiO_3 solution. The activator/binder ratio is 0.5. The Na_2O content is 4.7% of the binder and the molar ratio (SiO_2/Na_2O) is 1.5. The water-to-solid ratio was therefore 0.344. The activator had a density of 1.23 g/ml. The activator/binder ratio and the composition of the activator was designed according to previous studies [23,44,45]. The activator was prepared at least one day before mixing so that the solution was cooled down to ambient temperature and the species in the activator equilibrated.

2.2. Mixtures

The mixture proportions of AAS and AASF paste and concrete are shown in Table 2. Because pure fly ash based AAMs does not set in a reasonable time in ambient temperature, it is not considered in this paper. The aggregate was river stone made from quartz and was in saturated surface-dry condition at the time of casting. The volume fractions of aggregate in AAS and AASF concrete are around 67%. All the mixtures in this study were cured in sealed condition at 20 °C.

3. Experimental

The experimentally measured autogenous shrinkage of AAC will be used to evaluate the accuracy of the models, which will be described in Section 4. The compressive strength of AAC and the autogenous shrinkage, elastic modulus, and reaction heat of alkali-activated paste will be used as inputs in the models. The tensile strength of AAC is needed in investigating the potential of microcracking. Hence, the experimental methods and results on these parameters are given first in this section before presenting the modelling methods and results.

3.1. Autogenous shrinkage of concrete

The autogenous shrinkage of AAC was measured by an Autogenous Deformation Testing Machine (ADTM) [46]. A detailed description of ADTM can be found in Ref. [47]. The prismatic concrete specimen had a size of 1000 × 150 × 100 mm^3. The length change of the concrete was measured by LVDTs with an accuracy within ±1 μm. The instalment of LVDTs was conducted at 8 h after casting when the concrete had reached sufficient strength to support the embedded measuring bars that were connected with the LVDTs. The concrete specimen was sealed by plastic foil and tapes to avoid moisture loss to the environment. The temperature of the core of the concrete was controlled at 20 °C by a cryostat through circulating water within the mould. The measurement was

Table 2
Mixture proportions of AAS and AASF paste and concrete (kg/m^3).

Mixtures	AAS paste	AASF paste	AAS concrete	AASF concrete
Slag	400	200	400	200
Fly ash	0	200	0	200
Activator	200	200	200	200
Aggregate [0 mm–4 mm]	–	–	789	789
Aggregate [4 mm–8 mm]	–	–	440	440
Aggregate [8 mm–16 mm]	–	–	525	525
Additives	–	–	–	–

Table 1
Properties of slag and fly ash.

	Oxide (wt. %)									Particle size (μm)			Density (g/cm^3)
	SiO_2	Al_2O_3	CaO	MgO	Fe_2O_3	SO_3	K_2O	TiO_2	Other	D10	D50	D90	
Slag	31.8	13.3	40.5	9.3	0.5	1.5	0.3	1.0	1.9	4.6	18.3	33.2	2.9
Fly ash	56.8	23.8	4.8	1.5	7.2	0.3	1.6	1.2	2.8	10.6	48.1	83.4	2.4

stopped at the age of 21 days since the specimen in a parallel measurement under fully restrained condition cracked at this age (the results and discussion on the cracking of AAC under restrained condition were published elsewhere [47]).

The measured autogenous shrinkage of AAC is shown in Fig. 1. The development of autogenous shrinkage of AASF concrete is slower than that of AAS concrete. Comparing the results in Fig. 1 with the results in the literature, we can see that the autogenous shrinkages of AAS and AASF concrete are higher than the autogenous shrinkage or even the drying shrinkage of commonly used OPC based concrete with w/b ranging from 0.26 to 0.52 [15,48,49]. However, the autogenous shrinkage of AAS and AASF concrete is lower than the drying shrinkage of slag and high-calcium fly ash based concrete [15,50].

3.2. Strength of concrete

The compressive strength and splitting tensile strength of the concrete were measured according to NEN-EN 12390 [51]. Concrete cubes ($150 \times 150 \times 150$ mm^3) were cast and cured in temperature-controlled steel moulds. The moulds were connected with cryostats and the upper surface was sealed by plastic film. The temperature of the concrete cubes was controlled at 20 °C. The measurements were conducted at the ages of 1, 3, 7, 28 days.

The compressive strength of AAS and AASF concrete is shown in Fig. 2 (a) [47]. AAS concrete shows higher compressive strength than AASF concrete. This is consistent with the positive correlation between mechanical properties and slag content in AAMs as identified in Refs. [44,52,53].

The splitting tensile strength of the concrete is shown in Fig. 2 (b). The splitting tensile strength of the two concrete mixtures express similar evolution trends as the compressive strength as shown in Fig. 2 (b). Despite the high compressive strength of AAS and AASF concrete, their tensile strength seems not higher than the normal tensile strength of OPC based concrete [54].

3.3. Autogenous shrinkage of paste

The autogenous shrinkage of AAS and AASF paste was measured according to ASTM C1968 [55]. The corrugated tubes had a diameter of 28.5 mm and a length of 425 mm including the plugs. The freshly mixed paste was cast into the tubes while being vibrated. The length change of the tube was measured by LVDTs with an accuracy within ±1 μm. The tubes were stored in glycol whose temperature was controlled at 20 ± 0.1 °C by a cryostat. Three specimens were measured for each mixture.

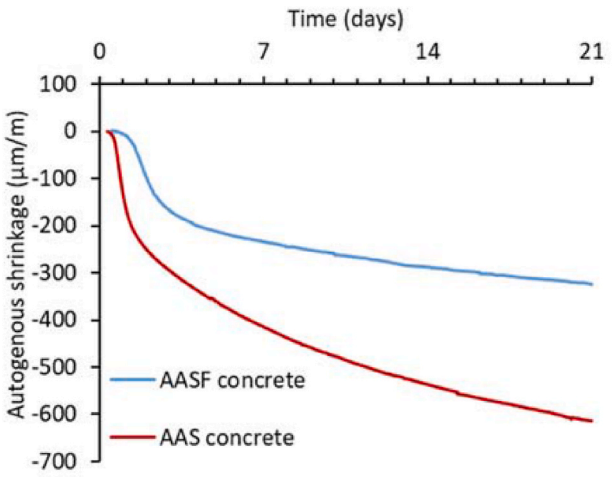

Fig. 1. Measured autogenous shrinkage of AAC. The measurements started at 8 h and 11 h for AAS and AASF concrete, respectively, when the concrete is stiff enough to hold the measuring bars [47].

The automatic measurements show a low scatter for triplicate samples, with the relative standard error in the range of 1–2% after the Vicat setting [56] of the pastes. The tests last 21 days as consistent with the autogenous shrinkage measurement on concrete.

The measured autogenous shrinkage of AAS and AASF paste is presented in Fig. 3. AAS paste shows larger autogenous shrinkage than AASF paste, which is consistent with the results on concrete (Fig. 1) and the findings of [57]. The discussion of the shrinkage mechanisms of AAS and AASF can be found in Ref. [14]. It is worth noting that even the autogenous shrinkage of AASF is already much higher than the common autogenous shrinkage of OPC based pastes, which is normally below 2000 μm/m in the first month of curing [17,58–60]. The autogenous shrinkage results on AAS and AASF pastes will be used as inputs to predict the autogenous shrinkage of AAC.

3.4. Elastic modulus of paste

The elastic modulus of the paste was measured automatically through EMM-ARM (which stands for 'Elasticity Modulus Monitoring through Ambient Response Method' [60]) from casting to 21 days. This method monitored continuously the first vibration frequency of the cantilevered beam composed of an acrylic tube with paste cast inside. The beam had a span of 450 mm and an outer diameter of 20 mm. The inner diameter of the acrylic tube, which was also the outer diameter of the paste, was 16 mm. The elastic modulus of the paste was then obtained from the vibration frequency, geometry and mass of the tube and the paste through the application of the dynamic equation of motion of the beam. Three samples were tested for each mixture. The measurements last for 21 days.

Fig. 4 shows the elastic modulus of the paste. The elastic modulus develops slowly in the first hours (8 h for AAS paste and 11 h for AASF paste), after which a rapid increase is observed for both pastes. From 7 days until 21 days, the increase in elastic modulus of the mixtures is minor. The magnitude of the 21-days elastic moduli of the pastes agrees with the results from Ref. [62], where the elastic modulus of AASF paste was measured according to static loading method. In comparison, the elastic moduli of AAMs based concrete are relatively higher, reaching more than 20 GPa at 28 days [47,63], probably due to the incorporation of aggregates which are much stiffer than the paste.

3.5. Reaction heat

A TAM Air isothermal calorimeter was used to measure the reaction heat of the paste in the first 7 days. The detailed measuring procedure can be found in Ref. [14].

The heat release from 7 days until the completion of the reaction was obtained by extrapolation through exponential models as shown in Equation (1) [64–66].

$$Q(t) = Q_{max} \exp\left[-\left(\frac{\mu}{t}\right)^{\alpha}\right] \quad (1)$$

where $Q(t)$ is the heat release at time t, Q_{max} is the ultimate heat at the completion of the reaction obtained by curve fitting, μ and α are the fitting parameters associated with the time and the shape of the exponential model.

Due to the difficulty of using one equation to fit multi-curvature evolutions, the reaction heat curves were fitted by a piecewise approximation with two functions. The measured and fitted reaction heat of the pastes is shown in Fig. 5. The parameters and the accuracy of the fitting are shown in Table 3.

From the reaction heat results, the reaction degree $\alpha(t)$ of the paste at a certain curing age can be calculated by Equation (2) [67]. Due to the same curing condition of the paste and concrete samples, the reaction degrees of the concrete are assumed identical to those of the pastes.

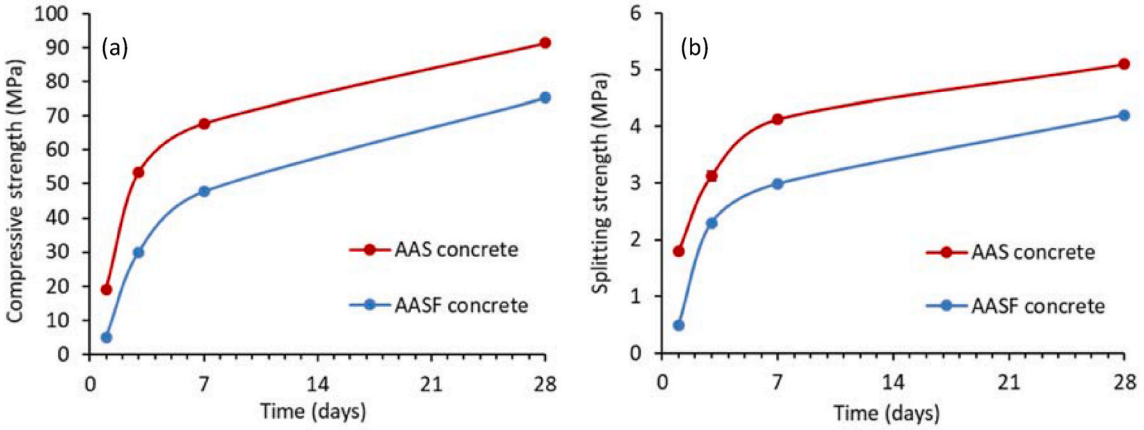

Fig. 2. Measured compressive (a) and splitting tensile (b) strength of AAS and AASF concrete.

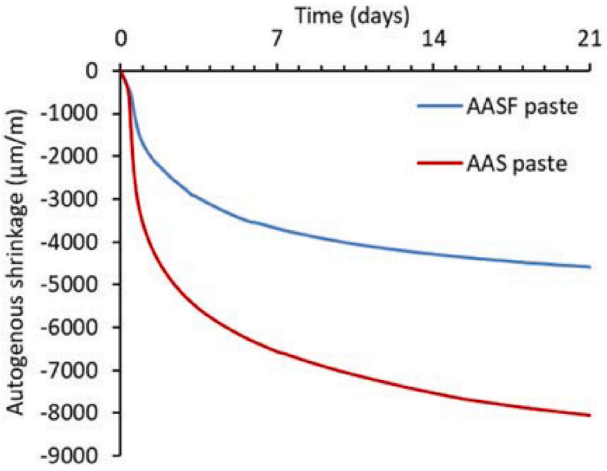

Fig. 3. Measured autogenous shrinkage of the paste. The measurements start at the Vicat setting times of the pastes determined by the Vicat method determined according to Ref. [61].

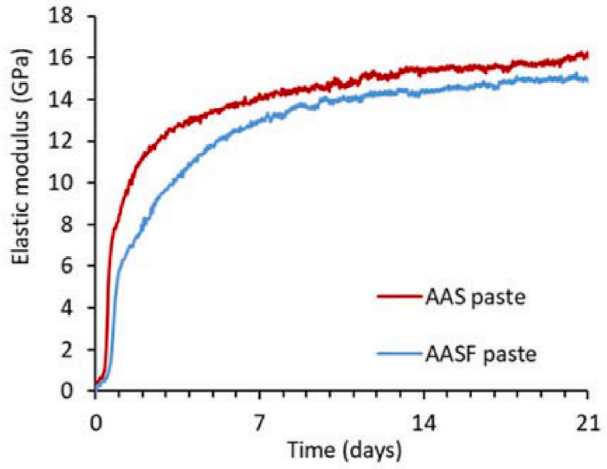

Fig. 4. Measured elastic modulus of alkali-activated paste.

$$\alpha(t) = \frac{Q(t)}{Q_{max}} \tag{2}$$

4. Evaluation of existing autogenous shrinkage models

In this section, the analytical expression MC2010 and Pickett's model are applied to predict autogenous shrinkage of AAC. The discrepancies between the predicted and measured results are discussed. Based on discussion, an extended Pickett's model is proposed to predict the autogenous shrinkage of AAC.

4.1. MC2010

According to MC2010, the autogenous shrinkage of concrete can be calculated according to Equation (3) [68].

$$\varepsilon_{cas}(t) = \varepsilon_{caso}(f_{cm}) \cdot \beta_{as}(t) \tag{3}$$

where $\varepsilon_{cas}(t)$ is the autogenous shrinkage at time t. f_{cm} is mean compressive strength of concrete cylinder at the age of 28 days. Note that the compressive strength shown in Fig. 2 was obtained on concrete cubes. To obtain cylinder compressive strength, a factor of 0.8 is needed according to Ref. [69]. $\varepsilon_{caso}(f_{cm})$ is expressed as shown in Equations (4) and (5) [68].

$$\varepsilon_{caso}(f_{cm}) = -\alpha_{as}\left(\frac{0.1 \times f_{cm}}{6 + 0.1 \times f_{cm}}\right)^{2.5} \cdot 10^{-6} \tag{4}$$

and

$$\beta_{as}(t) = 1 - exp\left(-0.2 \cdot t^{0.5}\right) \tag{5}$$

where α_{as} is a factor determined by the type of paste. α_{as} = 800, 700 or 600, for slowly hardening cements, normal or rapidly hardening cements, or rapidly hardening high strength cements, respectively. Since AAS and AASF show fast setting [23] and high strength [70], the coefficient α_{as} is chosen as 600 for both systems.

According to Equations (3)–(5), the autogenous shrinkage of AAC is calculated and compared with experimental data as shown in Fig. 6. It is found that the calculated autogenous shrinkage is only 12% of the measured results for both AAS and AASF concrete. The huge discrepancy reveals that the analytical model for autogenous shrinkage calculation in MC2010 that was designed for OPC is not applicable for AAC. The empirical parameters involved in Equations (3)–(5) were obtained based on a vast amount of experimental results on the compressive strength and autogenous shrinkage of OPC based concrete. For AAMs, which have intrinsically different compositional and microstructural properties, the mechanism of the autogenous shrinkage is different [14]. Thus

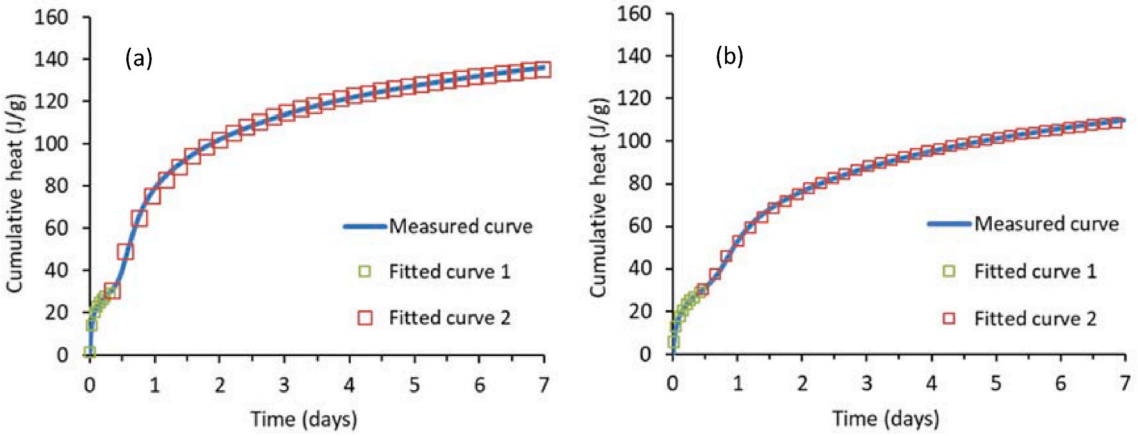

Fig. 5. Measured and fitted reaction heat of (a) AAS and (b) AASF pastes.

Table 3
Fitting parameters of the exponential models for the heat release of AAS and AASF pastes [47].

	Q_{max}	α	μ	R-square
Fitted curve 1 for AAS	–	0.33	1.98	0.998
Fitted curve 2 for AAS	155.04	0.49	23.68	0.998
Fitted curve 1 for AASF	–	0.22	44.02	0.999
Fitted curve 2 for AASF	139.13	0.47	46.04	0.999

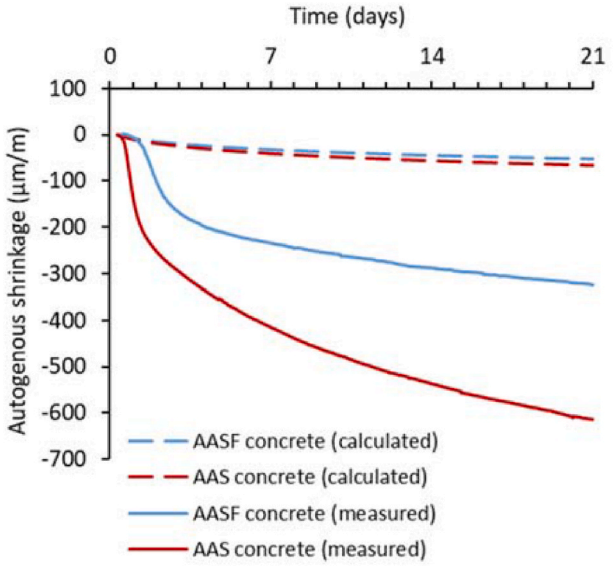

Fig. 6. Calculated autogenous shrinkage according to MC2010 (dashed lines) compared with the measured autogenous shrinkage (solid lines).

the relationship between compressive strength and autogenous shrinkage ought to differ too. New expressions, at least new empirical parameters, are needed for the establishment of analytical models for AAC. To achieve this, dramatically experimental efforts on AAMs seem inevitable, especially considering the larger variety in the precursors and activators that can be used to synthesize AAMs.

4.2. Pickett's model

4.2.1. Theory

In this section, the theory background of Pickett's model will be described, since the equation derivation will be the base of the extension in the next section. In Pickett's model [33], concrete is considered as composed of two phases, i.e. aggregates and paste. The paste is treated as homogeneous and elastic material, while the aggregate is considered as elastic spherical particle which embeds in a large body of shrinking paste. The restraining effect of one aggregate on the shrinking paste shell is calculated first. The sum of the restraining effect of all aggregates together determines the reduction in overall shrinkage of the paste. In the derivation, the restraining effect of each particle on the shrinking paste is assumed to be the same for each particle and independent from each other.

The shrinkage of the paste shell causes the following stresses as shown in Equations (6) and (7) [71,72]. A schematic diagram of the restraining effect is presented in Fig. 7.

$$\sigma_r = -\frac{p\mathrm{a}^3}{r^3}\frac{b^3 - r^3}{b^3 - \mathrm{a}^3} \tag{6}$$

$$\sigma_t = \frac{p\mathrm{a}^3}{2r^3}\frac{b^3 + 2r^3}{b^3 - \mathrm{a}^3} \tag{7}$$

where σ_r is the normal stress in the radial direction. a is the radius of the inner aggregate particle. b is the radius of outer shell. σ_t is the normal stress perpendicular to the radius. p is the pressure between inner and outer spheres. r is the radial coordinate.

The change of radius δ_r of the paste shell due to the presence of inner sphere can be calculated by Equation (8) [33] (a schematic diagram is shown in Fig. 8):

$$\delta_r = \frac{r}{E_p}\left[(1-\vartheta_p)\sigma_t - \vartheta_p\sigma_r\right] \tag{8}$$

The volume reduction of the total body is decreased by the amount:

$$4\pi b^2\delta_r|_{r=b} = \frac{3pV_a}{E_p}\left(\frac{1-\vartheta_p}{2}\right)\frac{3b^3}{b^3 - \mathrm{a}^3} \tag{9}$$

where $V_a = 4\pi\mathrm{a}^3/3$ is the volume of the inner particle, i.e. aggregate.

If the inner restraint is not present, the outer sphere would have reduced by a volume of $3\varepsilon V$, where ε is the unit linear shrinkage and V is the total volume. The decrease in volume shrinkage due to the presence of aggregate can be expressed as $-3\Delta\varepsilon V$, where $\Delta\varepsilon$ is the decrease in the linear shrinkage:

$$-3\Delta\varepsilon V = 4\pi b^2\delta_r|_{r=b} = \frac{3pV_a}{E_p}\left(\frac{1-\vartheta_p}{2}\right)\frac{3b^3}{b^3 - \mathrm{a}^3} \tag{10}$$

Another expression containing the pressure p can be found by considering the compressibility of the restraining particle. Reduction in volume of the inner aggregate caused by the pressure p on it can be calculated by:

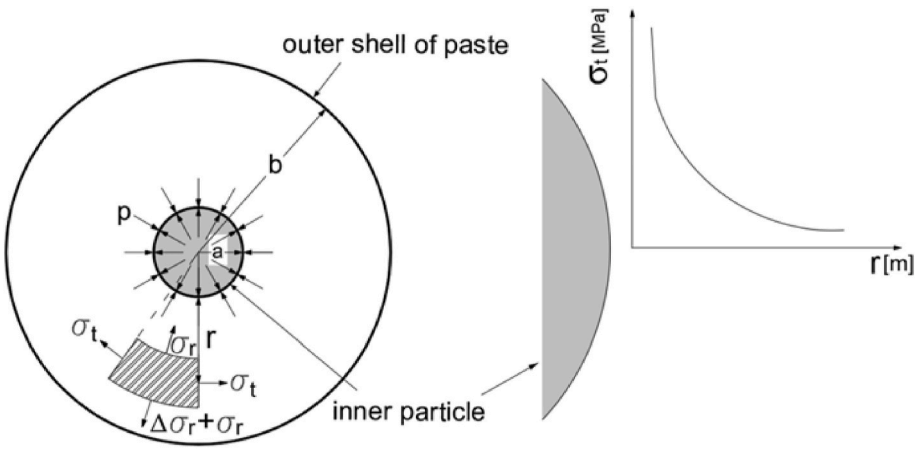

Fig. 7. Schematic representation of (left) restraining effect of aggregate on shrinking paste (after [73]) and (right) relationship between radius r and stress σ_t.

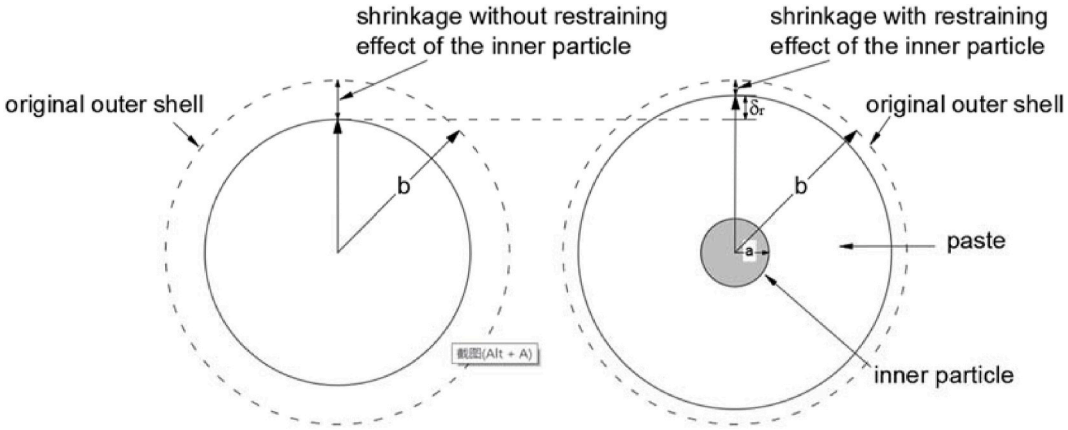

Fig. 8. Schematic representation of change of the radius of the outer paste shell due to the restraining of the inner particle, i.e. aggregate (after [73]).

$$\frac{3(1-2\vartheta_a)pV_a}{E_a} = 3\varepsilon V_a - 4\pi a^2 \delta_r|_{r=a} \tag{11}$$

where E_a and ϑ_a are is the elastic modulus and the Poisson ratio of the aggregate, respectively.

Eliminating p in Equations (10) and (11) (according to Pickett, the b/a is taken as ∞ [33]), we have:

$$-\Delta\varepsilon V = \beta\varepsilon V_a \tag{12}$$

where

$$\beta = \frac{3(1-\vartheta_p)}{1+\vartheta_p+2(1-2\vartheta_a)E_p/E_a} \tag{13}$$

The elastic modulus (E_p) of AAS and AASF paste has been shown in Fig. 4. The elastic modulus of the aggregate is 76 GPa (a common value for quartz). The Poisson ratio of paste and aggregate can be taken as 0.2 [74] and 0.25 [75], respectively. With these parameters, the factor β can be obtained by Equation (13).

Now that the restraining effect of one aggregate on the shrinking paste has been described, the sum of the restraining effect of all aggregates with a volume ratio of Φ_A can be calculated. When one more aggregate particle with volume V_a is added into the concrete, the change of the total volume ratio of aggregate Φ_A can be calculated as Equation (14) [33].

$$\Delta\Phi_A = \frac{\Phi_A V + V_a}{V+V_a} - \Phi_A = (1-\Phi_A)\frac{V_a}{V+V_a} \tag{14}$$

From Equations (12) and (14), we get:

$$\frac{\Delta\varepsilon}{\varepsilon} = -\frac{\beta\Delta\Phi_A}{1-\Phi_A}\frac{V+V_a}{V} \tag{15}$$

$$\frac{d\varepsilon}{\varepsilon} = -\frac{\beta d\Phi_A}{1-\Phi_A} \tag{16}$$

$$\varepsilon_c = \varepsilon_p(1-\Phi_A)^\beta \tag{17}$$

where ε_c is the autogenous shrinkage of concrete. ε_p is the autogenous shrinkage of paste. The autogenous shrinkage of AAS and AASF paste has been shown in Fig. 3. The volume ratio of the aggregate, Φ_A, is 67% for the AAC studied in this paper.

4.2.2. Calculated results and discussion

According to Equation (17), the autogenous shrinkage of AAS and AASF concrete is calculate as shown in Fig. 9. The calculated autogenous shrinkage is much higher than the measured one in the whole period studied for both concrete mixtures.

One important reason of these discrepancies is believed to be the ignorance of creep in Pickett's model. As described in section 4.2.1, Pickett's model is derived according to classic elastic mechanics, with the assumption that aggregate and paste both behave elastically. However, in reality, the paste made from either OPC or AAMs shows a certain extent of viscosity. A part of the autogenous shrinkage of the paste belongs to time-dependent deformation under internal driving forces, viz. creep. It has been found in a previous study [14] that the creep coefficients of AAS and AASF pastes can reach 3–4, which are much higher

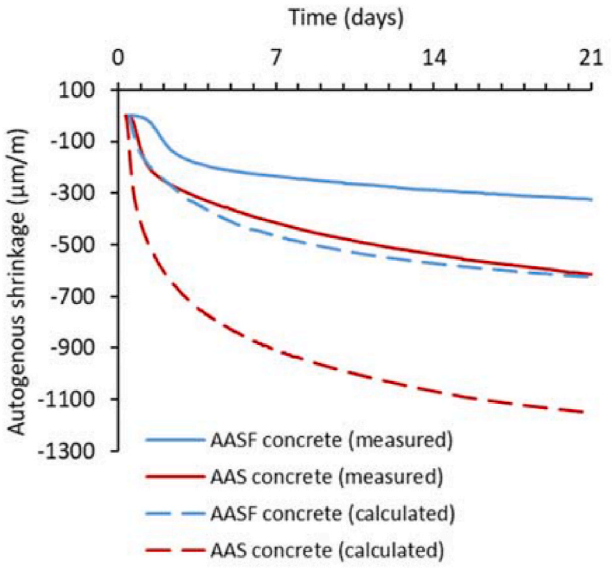

Fig. 9. Calculated autogenous shrinkage according to Pickett's model (dashed lines) in comparison with the measured autogenous shrinkage (solid lines).

than those for OPC systems. Furthermore, with the increase of time, the role of creep will be increasingly important. Whereas, the restraining effects of aggregate on elastic deformation and creep of the paste might not be identical. According to Ref. [30], the embedding of stiff particles restrains more effectively the viscous deformation than the elastic deformation of the paste. Therefore, considering all the deformation of AAC as elastic would underestimate the restraining effect of the aggregate. It has been found that the more aggregate contained in the concrete, the higher the discrepancy between the calculated and measured autogenous shrinkage will be generated by Pickett's model [43]. Therefore, for a better prediction of the autogenous shrinkage of the concrete that contains a big amount of aggregate, the creep has to be considered.

Lura and Wyrzykowski [30] suggested to use a reduced elastic modulus of the paste or an increased elastic modulus of the aggregates to practically consider the effect of creep. In either way, a smaller $E_p/\ E_a$ can be expected, which would result in a stronger restraining effect of aggregate on the shrinking paste as illustrated in Fig. 8. However, artificially choosing a reduced elastic modulus of the paste, for example using an effective modulus of 1/3 of the measured one as suggested by Ref. [76], can be somehow arbitrary. Besides, a constant value of elastic modulus, although reduced, cannot reflect the time-dependent characteristics of creep. For a better estimation of the autogenous shrinkage of the concrete, the accumulative effect of creep needs to be considered, as will be shown in the next section.

5. Prediction of autogenous shrinkage of AAC by Extended Pickett's model

4.3. Theory

As discussed in the last section, creep plays an important role in the autogenous shrinkage of AAMs paste. Pickett's model assumes the deformation of the paste as purely elastic, thus showing a large discrepancy in prediction. To better predict the autogenous shrinkage of AAC, the restraining effects of aggregate on both the elastic and creep deformations need to be considered. To do that, an extension of Pickett's model can be made to integrate creep into the current equations.

Firstly, the total autogenous shrinkage of paste is considered to include two parts, i.e. an elastic part and a creep part.

$$\varepsilon_p = \varepsilon_{p,\ el} + \varepsilon_{p,cr} \tag{18}$$

where ε_p is the measured autogenous shrinkage of the paste. $\varepsilon_{p,el}$ and $\varepsilon_{p,cr}$ are the elastic and creep parts of the autogenous shrinkage, respectively.

As found in a previous study [14], the creep coefficient proposed by van Breugel [77] provides a good prediction of the creep of AAS and AASF pastes, as shown in Equations (19) and (20).

$$\varepsilon_{cr}(t,\tau) = \varepsilon_{el}(\tau)\phi(t,\tau) \tag{19}$$

$$\phi(t,\tau) = \left(\frac{\alpha(t)}{\alpha(\tau)} - 1\right) + 1.34{*}\omega^{1.65}\tau^{-d}(t-\tau)^n\frac{\alpha(t)}{\alpha(\tau)} \tag{20}$$

where $\phi(t,\tau)$ is the creep coefficient. τ (days) is the time when the load is applied. ω is the water-solid ratio, 0.344 in the case of this study (see section 2.1). α is the degree of reaction. n and d are constants which value is taken as 0.3 and 0.35, respectively [14,78].

In Equation (20), the ratio of reaction degree $\frac{\alpha(t)}{\alpha(\tau)}$ can be obtained by using the reaction heat $Q(t)$ as:

$$\frac{\alpha(t)}{\alpha(\tau)} = \frac{Q(t)}{Q(\tau)} \tag{21}$$

The reaction heat results can be found in Fig. 5.

The creep part at a certain time is the accumulation of increments of time-dependent deformations that formed at previous time, e.g. from τ_1 to τ_{n-1}:

$$\varepsilon_{cr}(t,\ \tau) = \sum_{k=1}^{n-1}\Delta\varepsilon_{el}\ (\tau_k)\left[\left(\frac{\alpha(t)}{\alpha(\tau_k)} - 1\right) + 1.34 * \omega^{1.65}\tau_k^{-d}(t-\tau_k)^n\frac{\alpha(t)}{\alpha(\tau_k)}\right] \tag{22}$$

According to Equations (18)–(22) and the measured autogenous shrinkage of the paste (see Fig. 3), the elastic part and creep part of the autogenous shrinkage of AAMs paste can be calculated.

As mentioned in section 4.2.1, aggregate in concrete will restrain the shrinking paste. The change of the radius of outer shell δ_r also consists two parts: an elastic part and a time-dependent part.

For the elastic part $\delta_{r,el}$, it holds (the same as Equation (8)):

$$\delta_{r,el} = \frac{r}{E_p}\left[(1-\vartheta_p)\sigma_t - \vartheta_p\sigma_r\right] \tag{23}$$

For the creep part $\delta_{r,cr}$, it holds:

$$\delta_{r,cr} = \frac{r}{E_p}\left[(1-\vartheta_p)\sigma_t - \vartheta_p\sigma_r\right]\left[\left(\frac{\alpha(t)}{\alpha(\tau)} - 1\right) + 1.34 * \omega^{1.65}\tau^{-d}(t-\tau)^n\frac{\alpha(t)}{\alpha(\tau)}\right] \tag{24}$$

From Equations (6), (7), (23) and (24), the change of radius of the outer shell δ_r can be calculated by summing $\delta_{r,el}$ and $\delta_{r,cr}$ (a and b as in Fig. 7):

$$\delta_r = \frac{p\mathrm{a}^3}{E_p r^2}\left[\frac{1-\vartheta_p}{2}\frac{b^3+2r^3}{b^3-\mathrm{a}^3} + \vartheta_p\frac{b^3-r^3}{b^3-\mathrm{a}^3}\right]\left[1 + \left(\frac{\alpha(t)}{\alpha(\tau)} - 1\right) + 1.34 * \omega^{1.65}\tau^{-d}(t-\tau)^n\frac{\alpha(t)}{\alpha(\tau)}\right] \tag{25}$$

The reduced volume shrinkage of the total body due to the restraint of aggregates is of the amount:

$$4\pi b^2\delta_r|_{r=b} = \frac{3pV_a}{E_p}\left(\frac{1-\vartheta_p}{2}\right)\frac{3b^3}{b^3-\mathrm{a}^3}\left[1 + \left(\frac{\alpha(t)}{\alpha(\tau)} - 1\right) + 1.34{*}\omega^{1.65}\tau^{-d}(t-\tau)^n\frac{\alpha(t)}{\alpha(\tau)}\right] \tag{26}$$

where $V_a = 4/3\pi\mathrm{a}^3$ is the volume of the aggregate.

The decrease in volume shrinkage due to the presence of aggregate $-3\Delta\varepsilon V$ can be written as:

$$-3\Delta\varepsilon V = \frac{3pV_a}{E_p}\left(\frac{1-\vartheta_p}{2}\right)\frac{3b^3}{b^3-\mathrm{a}^3}\left[1 + \left(\frac{\alpha(t)}{\alpha(\tau)} - 1\right) + 1.34{*}\omega^{1.65}\tau^{-d}(t-\tau)^n\frac{\alpha(t)}{\alpha(\tau)}\right] \tag{27}$$

The volume reduction of the aggregate due to the force p has been

shown in Equation (10). Eliminating p in Equations (27) and (11):

$$-\Delta\varepsilon V = \beta_{\varnothing}\varepsilon V_a \tag{28}$$

where

$$\beta_{\varnothing} = \frac{3(1-\vartheta_p)}{1+\vartheta_p+2(1-2\vartheta_a)(E_p/E_a)\Big/\left[1+\left(\frac{\alpha(t)}{\alpha(\tau)}-1\right)+1.34*\omega^{1.65}\tau^{-d}(t-\tau)^{n\frac{\alpha(t)}{\alpha(\tau)}}\right]} \tag{29}$$

The relationship between the shrinkage of paste and corresponding concrete can be then calculated as:

$$\varepsilon_c = \varepsilon_p(1-\Phi_A)^{\beta_{\varnothing}} \tag{30}$$

where ε_c is the autogenous shrinkage of concrete. ε_p is the autogenous shrinkage of paste (see Fig. 3). The factor $\beta_{\varnothing}$ evolves with time (see Equation (29)).

4.4. Calculated results and discussion

With the extended Pickett's model, the autogenous shrinkage of AAS and AASF concrete is calculated and shown in Fig. 10. It is seen that the extended Pickett's model with creep taken into account provides a much better prediction of the autogenous shrinkage of AAC than the original Pickett's model. The mechanism behind lies in the separate consideration of the elastic and creep deformations of the paste and on the latter one, aggregates have more significant restraining effects (see Equations (23) and (24)).

In the first 7 days, the extended Pickett's model overestimates the autogenous shrinkage of both AAS and AASF concrete. The main reason for this is believed to lie in the slightly different curing conditions of the paste and concrete samples. Nominally, isothermal curing conditions were applied on the measurements of both paste and concrete samples. In fact, however, the temperature controlling strategies in the two experiments are different. As described in section 3.3, it is the temperature of the liquid where the paste samples were stored that is under control. Due to the hydration heat, the core part of the paste would be slightly hotter than the edge part of the corrugated tube that contacts the liquid. Therefore, the average temperature of the paste would be a bit higher than 20 °C, despite the small cross-section of the corrugated tube. By contrast, in the concrete measurement, it is the temperature of the core part of the concrete that is measured and controlled. The concrete sample has a large cross-section, 150 × 100 mm^2. While the temperature of the core part of the concrete was accurately controlled at 20 °C, the temperature of the edge parts of concrete must be below 20 °C, since they are closer to the mould, which has cooling water circulating inside to remove the reaction heat. Hence, there was actually a temperature gradient within the cross-section of the concrete sample and the average temperature of the whole concrete is below 20 °C. A schematic diagram of the temperature gradient is presented in Fig. 11. This gradient is considerable mainly in the first day when the reaction was generating huge amounts of heat (see Fig. 5). In fact, the temperature of the circulating water was as low as 5–10 °C in the first hours in order to cool down the concrete. Due to the actually lower curing temperature of the concrete samples, the reactions would be retarded a bit at the very early age compared to those of the paste and there would be a longer dormant period. Therefore, the development of the autogenous shrinkage of the concrete would be slowed down in the first 1–2 days, thus becomes lower than the predicted autogenous shrinkage based on the results of the paste.

Despite the effects discussed above, the discrepancy between the measured and calculated results is within 9% for AAS concrete in the period studied. For AASF concrete, the measured and calculated curves nearly overlap with each other after the first 3 days. These results reveal that it is necessary to consider creep in order to accurately predict the autogenous shrinkage of AAC.

The small discrepancy shown in Fig. 10 indicates that the model proposed here can well estimate the creep of AAMs, which accounts for a significant part of the autogenous shrinkage. Regarding the mechanism

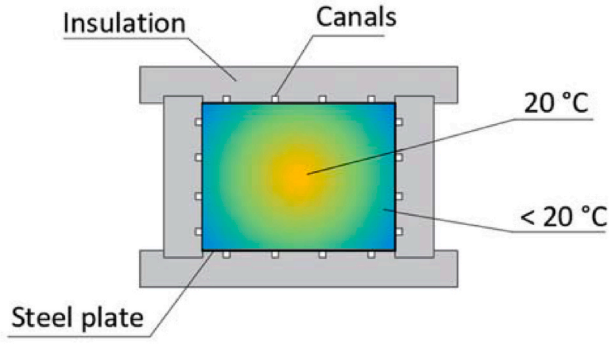

Fig. 11. A schematic diagram of the temperature gradient within the concrete cured in ADTM.

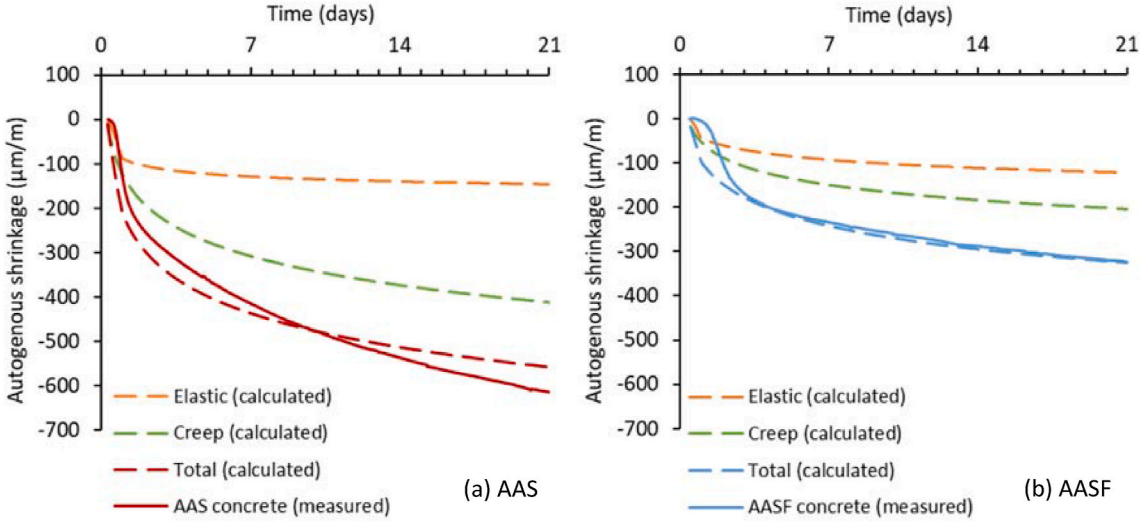

Fig. 10. Calculated autogenous shrinkage of AAS concrete (a) and AASF concrete (b) according to the extended Pickett's model (dashed lines) compared to the measured autogenous shrinkage (solid lines).

behind the pronounced creep of AAMs, Ye and Radlińska [24] mentioned that it may originate from the viscosity of C-A-S-H gel due to the reduced stacking regularity by the incorporation of alkali cations, which makes the gel easier to collapse or redistribute. This might be true, but the results from this study suggest that the large creep deformation of AAMs should be also related to the reaction kinetics of the materials, as shown in Equation (20). The key factor appears not the absolute reaction degree, but the $\alpha(t)/\alpha(\tau)$ ratio, which indicates the evolution of reaction degree from time τ to time t. For example, the reaction degree of OPC at 3 days normally can reach 70–80% of that at 28 days [79,80]. For AAMs, by contrast, the reaction degree can double from 3 days to 28 days [81]. In that case, a higher $\alpha(t)/\ \alpha(\tau)$ would be obtained for AAMs, thus a larger creep at 28 days under the load, which starts at 3 days, e.g. capillary tension, according to Equation (20). In other words, the large autogenous shrinkage of AAMs might be partially due to the relatively slow reaction in early age. The continuous increment of reaction degree afterwards objectively provides longer time for the material to deform. For OPC based system, a high reaction degree can be reached in the first days, which also ensures a fast gain of stiffness (see Ref. [82]) that can resist the development of creep. This inference might be useful for a better understanding towards the large creep and large autogenous shrinkage of AAC.

The extended Pickett's model proposed herein can act as a handy tool for industry and researchers to predict the autogenous shrinkage of AAC from the autogenous shrinkage of corresponding paste. Of course, this study only covers the currently commonly used AAMs based on slag/fly ash with NaOH and Na_2SiO_3 as the activator. The applicability of the model to AAMs made from other precursors and activators needs further research.

5. Evaluation of microcracking surrounding the aggregates

Since the shrinkage of paste is restrained by the aggregate, tensile stress would be generated in the paste. Consequently, microcracks that are perpendicular to the interface may form, as demonstrated in Fig. 12 [83].

The development of microcracking has severe influences on the mechanical properties of the concrete. As reported in Refs. [47,70], the development of microcracking is hypothesized to be responsible for the decrease in elastic modulus and tensile strength-to-compressive strength ratios of AAC. Moreover, the large scatter in the measured flexural strength observed by Nedeljković et al. [23] was also attributed to the microcracking caused by locally restrained autogenous shrinkage. Despite the plausible reasoning in these studies, none of them gave direct or indirect evidence on the microcracking.

Based on the Extended Pickett's model developed in section 5, the interactive forces between the aggregate and the paste can be calculated, which makes it possible to evaluate the potential of microcracking.

As shown in Fig. 7, the stresses perpendicular to the radius σ_t decreases with the increase of r. When r = a, i.e. at the surface of the aggregate, σ_t reaches the largest and can be calculated with equations (6) and (7) as:

$$\sigma_t = \frac{\varepsilon_p E_p \left(b^3 + 2a^3\right)}{2\left[\left(1-2\vartheta_p\right)a^3 - \left(1+\vartheta_p\right)b^3\right]} \tag{31}$$

According to Pickett, the b/a is taken as ∞ [33], hence we have:

$$\sigma_t = \frac{\varepsilon_p E_p}{-2\left(1+\vartheta_p\right)} \tag{32}$$

Due to the pronounced viscoelasticity of the material, the tensile stress generated in restrained paste would be reduced with the elapse of time, i.e. relaxation, which has to be considered when predicting the stress evolution [85]. According to van Breugel [77], a relaxation factor can be introduced to consider the effect of relaxation.

$$\sigma_{t-relax}(t,\ \tau) = \sigma_t(\tau)\psi(t,\ \tau) \tag{33}$$

where $\psi(t,\tau)$ is the relaxation factor. τ (days) is the starting time of the loading.

The relaxation coefficient of concrete can be calculated from the creep coefficient $\phi(t,\tau)$, as shown in Equation (34) [77,86].

$$\psi(t,\tau) = e^{-\phi(t,\tau)} \tag{34}$$

Since the autogenous shrinkage of surrounding cement paste is increasing with time, the relaxation of stress caused by restraining particles $\sigma_t(\tau)$ can be expressed as:

$$\sigma_{t-relax}(t) = \sum_{k=1}^{n-1} \Delta\sigma_{t-relax}(\tau_k) = \sum_{k=1}^{n-1} \Delta\sigma_t(\ \tau_k)\psi(t,\ \tau_k) \tag{35}$$

where $\Delta\sigma_{t-relaxed}(\tau_k)$ is the increment of elastic shrinkage-induced stress after relaxation from τ_{k-1} to τ_k.

Fig. 13 shows the predicted tensile stress at the surface of aggregate particle with and without consideration of relaxation in AAS and AASF concrete. It can be seen that the calculate stress in AAS concrete is higher than in AASF concrete, which is in line with the higher autogenous shrinkage of AAS concrete. The calculated tangential tensile stress is decreased by more than a half when relaxation is considered.

When the tensile stress is bigger than the tensile strength of the paste, microcracking will occur. The occurrence of microcracking of AAS and AASF concrete is calculated and also shown in Fig. 13, where the tensile

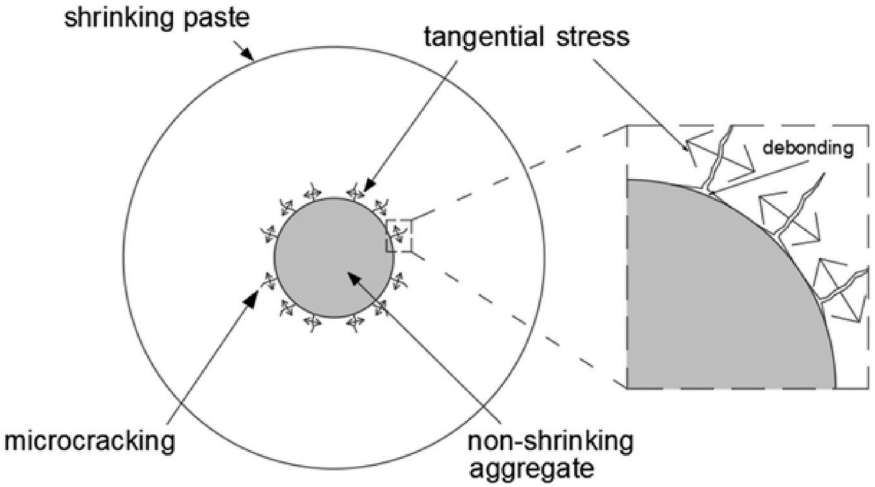

Fig. 12. Schematic representation of the microcracking generated on the interface of the shrinking paste and the inert particle (after [84]).

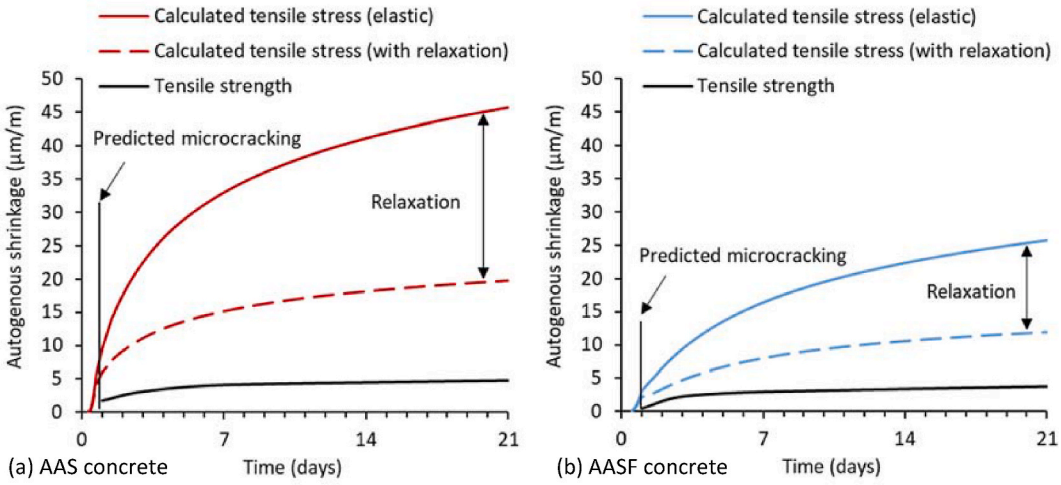

Fig. 13. Calculated tangential tensile stress with (dashed lines) and without (solid lines) consideration of relaxation in AAS concrete (a) and AASF concrete (b). The stress is compared with the measured tensile strength of AAS and AASF concrete strength (solid black lines, see Fig. 2 (b)). The calculated tensile stress appears higher than the tensile strength at 1 day of curing, as marked by the arrow.

strength of the paste is assume to be identical to that of the concrete (see Fig. 2). It is found that the calculated stress in AAC exceeds the tensile strength in only 1 day.

In reality, the development of microcracking may not be as early as 1 day, especially for AASF concrete, since the autogenous shrinkage of AAC in the first days was overestimated (see Fig. 10). Afterwards, nonetheless, the calculated stress in AAS and AASF concrete keeps increasing and becomes much higher than the measured tensile strength. This indicates a high potential of microcracking development in these two concrete mixtures in this period. Besides, it needs to be noted that the calculation of the tangential stress described above does not consider the overlapping of stress. In concrete, the stress fields generated in the paste due to the presence of multiple aggregates will overlap. If we take the overlap into account, the calculated tensile stress in the paste will be even larger. Compared to the results in Ref. [43], the tendency of microcracking in AAC is higher than that in OPC based concrete/mortar. The microcracking development numerically identified in this study may help to explain the decreased elastic modulus and tensile/flexural strength of AAMs based paste and concrete observed in previous studies [23,47,70].

One may argue that the splitting tensile strength of concrete is improper to be used here for the evaluation since it is not identical to the tensile strength of the paste surrounding aggregates. This is probably true, but there is currently no standard way to measure the tensile strength of paste; moreover, none of the commonly used means to break the paste, including uniaxial tension, splitting tension and 3-point/4-point bending, can fully mimic the failure of the paste surrounding aggregates due to tangential tensile stress. Lattice-type models might be useful to analyse the microcracking of paste under a complex loading conditions [87], but a challenge exists in giving viscoelastic constitution to the discrete beams of the mesh. Future studies to solve this problem are recommended.

It is also worth noting that the restraining effect of aggregate is not the exclusive cause of microcracking. Unreacted particles in paste are also local restraints of the shrinkage and may aggravate the development of microcracking, but that part is not considered in this study, where the paste is considered as a homogeneous material. Further research on the restraining effect of unreacted particles is needed, bearing in mind that a more complex situation is to be expected due to the much more irregular shape of the precursors than the aggregate, which may induce heterogeneous stress distribution, viz. stress concentration surrounding the particles. In addition, the influence of the particle size of the restraints including gravels, sand and unreacted models is not considered in the proposed model and can be an interesting topic for future studies.

6. Final remarks

There is a good connection between this paper and two companion papers [14,47] published recently. The former one deals with the prediction of the autogenous shrinkage of AAMs paste based on the internal relative humidity, elastic modulus, reaction degree, etc. of the paste. The latter one investigates the prediction of stress in restrain concrete based on the autogenous shrinkage of the concrete. By combining the approaches proposed in these three studies, it is theoretically possible to predict the cracking potential and stress of restrained AAC from the properties of corresponding paste, without even an autogenous shrinkage measurement. This will undoubtedly contribute to the establishment of model code for AAC. Of course, the more models and the less experimental evidence get involved, the larger prediction error might be expected. Future study is needed on integrating the models on different scales of the materials and improving the accuracy.

7. Conclusions

In this study, the autogenous shrinkage of AAC is predicted explicitly by considering the creep effect. The potential of microcracking surrounding aggregates is evaluated. According to the results and discussion, the following conclusions can be drawn:

1. While various models are available for OPC concrete, these models are likely not applicable for AAC. The model from MC2010 significantly underestimates the autogenous shrinkage of AAC. The empirical parameters designed for OPC concrete are not suitable for AAC. Pickett's model tends to overestimate the autogenous shrinkage of AAC and the discrepancy increases with the increase of slag content. One main reason of the discrepancy is attributed to the ignorance of the creep involved in the autogenous shrinkage of AAC.
2. To better predict the autogenous shrinkage of AAC, a new numerical model is developed by extending Pickett's model to consider the pronounced viscoelasticity of AAM paste. By this model, the restraining effects of aggregate on the elastic and creep deformations of the paste can be investigated separately. The modelling results by the extended Pickett model agree well with the measured results. Although the model is developed for AAC, it can be used for any other concrete whose creep cannot be ignored.

3. The microcracking in AAC due to the restraining effect of aggregate on the shrinkage of paste is evaluated. The calculated results indicate that AAC undergoes high potential of microcracking. This finding may help to explain the unexpected deterioration of the mechanical properties of AAC observed in previous studies.
4. The results in this study indicate that the role of aggregate in AAC is both positive and negative. From the autogenous shrinkage point of view, the aggregate restrains effectively the deformation of the paste especially the creep part of the autogenous shrinkage, thus resulting in a relatively low autogenous shrinkage of the concrete; on the other hand, the restraining effect induces a high tangential tensile stress in paste surrounding aggregates. Although the stress is reduced thanks to the pronounced relaxation, the tendency of microcracking in AAC is still high. The root reason originates from the very large autogenous shrinkage of AAMs pastes. Future study should be devoted to mitigating the autogenous shrinkage of AAMs pastes, in order to produce AAC with lower potential of microcracking.

CRediT authorship contribution statement

Zhenming Li: Conceptualization, Methodology, Investigation, Writing - original draft. **Tianshi Lu:** Conceptualization, Methodology, Software, Writing - original draft. **Yun Chen:** Investigation. **Bei Wu:** Investigation. **Guang Ye:** Project administration, Supervision, Writing - review & editing.

Declaration of competing interest

The authors declare that they have no known competing financial interests or personal relationships that could have appeared to influence the work reported in this paper.

Acknowledgment

Zhenming Li, Tianshi Lu and Yun Chen would like to acknowledge the funding supported by the China Scholarship Council (CSC) under grant No. 201506120072, No. 2011671058 and No. 201906150022, respectively. Zhenming Li would also like to thank the funding from Netherlands Organisation for Scientific Research (NWO).

References

[1] C. Shi, A.F. Jiménez, A. Palomo, New cements for the 21st century: the pursuit of an alternative to Portland cement, Cement Concr. Res. 41 (2011) 750–763, https://doi.org/10.1016/j.cemconres.2011.03.016.
[2] E. Worrell, L. Price, N. Martin, C. Hendriks, L.O. Meida, Carbon dioxide emissions from the global cement industry, Annu. Rev. Energy Environ. 26 (2001) 303–329.
[3] F. Pacheco-Torgal, Z. Abdollahnejad, S. Miraldo, M. Kheradmand, Alkali-activated Cement-Based Binders (AACBs) as Durable and Cost-Competitive low-CO2 Binder Materials: Some Shortcomings that Need to Be Addressed, Butterworth-Heinemann, Oxford, UK, 2017.
[4] J.L. Provis, Alkali-activated materials, Cement Concr. Res. 114 (2018) 40–48, https://doi.org/10.1016/j.cemconres.2017.02.009.
[5] S. Zhang, A. Keulen, K. Arbi, G. Ye, Waste glass as partial mineral precursor in alkali-activated slag/fly ash system, Cement Concr. Res. 102 (2017) 29–40, https://doi.org/10.1016/j.cemconres.2017.08.012.
[6] S. Yan, K. Sagoe-Crentsil, Properties of wastepaper sludge in geopolymer mortars for masonry applications, J. Environ. Manag. 112 (2012) 27–32, https://doi.org/10.1016/j.jenvman.2012.07.008.
[7] A. Fernández-Jiménez, A. Palomo, D. Revuelta, Alkali activation of industrial by-products to develop new Earth-friendly cements, NOMAT 2009, Proceeding 11th Int. Conf. Non-Conventional Mater. Technol. (2009) 1–15.
[8] K. Arbi, M. Nedeljković, Y. Zuo, G. Ye, A review on the durability of alkali-activated fly ash/slag systems: advances, issues, and perspectives, Ind. Eng. Chem. Res. 55 (2016) 5439–5453, https://doi.org/10.1021/acs.iecr.6b00559.
[9] X. Gao, Q.L. Yu, H.J.H. Brouwers, Reaction kinetics, gel character and strength of ambient temperature cured alkali activated slag-fly ash blends, Construct. Build. Mater. 80 (2015) 105–115, https://doi.org/10.1016/j.conbuildmat.2015.01.065.
[10] Y. Ding, J.G. Dai, C.J. Shi, Mechanical properties of alkali-activated concrete: a state-of-the-art review, Construct. Build. Mater. 127 (2016) 68–79, https://doi.org/10.1016/j.conbuildmat.2016.09.121.
[11] J. Zhang, C. Shi, Z. Zhang, Z. Ou, Durability of alkali-activated materials in aggressive environments: a review on recent studies, Construct. Build. Mater. 152 (2017) 598–613, https://doi.org/10.1016/j.conbuildmat.2017.07.027.
[12] G.J.G. Gluth, K. Arbi, S.A. Bernal, D. Bondar, A. Castel, S. Chithiraputhiran, A. Dehghan, K. Dombrowski-Daube, A. Dubey, V. Ducman, K. Peterson, P. Pipilikaki, S.L.A. Valcke, G. Ye, Y. Zuo, J.L. Provis, RILEM TC 247-DTA round robin test: carbonation and chloride penetration testing of alkali-activated concretes, Mater. Struct. Constr. 53 (2020) 1–17, https://doi.org/10.1617/s11527-020-1449-3.
[13] J.L. Provis, K. Arbi, S.A. Bernal, D. Bondar, A. Buchwald, A. Castel, S. Chithiraputhiran, M. Cyr, A. Dehghan, K. Dombrowski-Daube, A. Dubey, V. Ducman, G.J.G. Gluth, S. Nanukuttan, K. Peterson, F. Puertas, A. van Riessen, M. Torres-Carrasco, G. Ye, Y. Zuo, RILEM TC 247-DTA round robin test: mix design and reproducibility of compressive strength of alkali-activated concretes, Mater. Struct. 52 (2019) 1–13, https://doi.org/10.1617/s11527-019-1396-z.
[14] Z. Li, T. Lu, X. Liang, H. Dong, J. Granja, M. Azenha, G. Ye, Mechanisms of autogenous shrinkage of alkali-activated slag and fly ash pastes, Cement Concr. Res. 135 (2020) 106107, https://doi.org/10.1016/j.cemconres.2020.106107.
[15] Z. Li, J. Liu, G. Ye, Drying shrinkage of alkali-activated slag and fly ash concrete; A comparative study with ordinary Portland cement concrete, Heron 64 (2019) 149.
[16] M. Mastali, P. Kinnunen, A. Dalvand, R. Mohammadi Firouz, M. Illikainen, Drying shrinkage in alkali-activated binders – a critical review, Construct. Build. Mater. 190 (2018) 533–550, https://doi.org/10.1016/j.conbuildmat.2018.09.125.
[17] P. Lura, Autogenous Deformation and Internal Curing of Concrete, Delft University of Technology, 2003.
[18] Z. Li, A. Kostiuchenko, G. Ye, Autogenous shrinkage-induced stress of alkali-activated slag and fly ash concrete under restraint condition, in: ECI (Ed.), Alkali Act. Mater. Geopolymers Versatile Mater. Offer. High Perform. Low Emiss., 2018, p. 24. Tomar.
[19] Z.C. Grasley, D.A. Lange, Modeling drying shrinkage stress gradients in concrete, Cem. Concr. Aggregates 26 (2004) 115–122, https://doi.org/10.1520/cca12302.
[20] N.K. Lee, J.G. Jang, H.K. Lee, Shrinkage characteristics of alkali-activated fly ash/slag paste and mortar at early ages, Cement Concr. Compos. 53 (2014) 239–248, https://doi.org/10.1016/j.cemconcomp.2014.07.007
[21] A.A. Melo Neto, M.A. Cincotto, W. Repette, Drying and autogenous shrinkage of pastes and mortars with activated slag cement, Cement Concr. Res. 38 (2008) 565–574, https://doi.org/10.1016/j.cemconres.2007.11.002.
[22] J.G. Jang, N.K. Lee, H.K. Lee, Fresh and hardened properties of alkali-activated fly ash/slag pastes with superplasticizers, Construct. Build. Mater. 50 (2014) 169–176, https://doi.org/10.1016/j.conbuildmat.2013.09.048.
[23] M. Nedeljković, Z. Li, G. Ye, Setting, strength, and autogenous shrinkage of alkali-activated fly ash and slag pastes: effect of slag content, Materials (Basel) 11 (2018) 2121, https://doi.org/10.3390/ma11112121.
[24] H. Ye, A. Radlińska, Shrinkage mechanisms of alkali-activated slag, Cement Concr. Res. 88 (2016) 126–135, https://doi.org/10.1016/j.cemconres.2016.07.001.
[25] G. Fang, H. Bahrami, M. Zhang, Mechanisms of autogenous shrinkage of alkali-activated fly ash-slag pastes cured at ambient temperature within 24 h, Construct. Build. Mater. 171 (2018) 377–387, https://doi.org/10.1016/j.conbuildmat.2018.03.155.
[26] Z. Li, M. Nedeljković, B. Chen, G. Ye, Mitigating the autogenous shrinkage of alkali-activated slag by metakaolin, Cem, Concr. Res. 122 (2019) 30–41, https://doi.org/10.1016/j.cemconres.2019.04.016.
[27] Z. Li, M. Wyrzykowski, H. Dong, J. Granja, M. Azenha, P. Lura, G. Ye, Internal curing by superabsorbent polymers in alkali-activated slag, Cement Concr. Res. 135 (2020) 106123, https://doi.org/10.1016/j.cemconres.2020.106123.
[28] H. Ye, C. Fu, A. Lei, Mitigating shrinkage of alkali-activated slag by polypropylene glycol with different molecular weights, Construct. Build. Mater. 245 (2020) 118478, https://doi.org/10.1016/j.conbuildmat.2020.118478.
[29] Z. Li, S. Zhang, X. Liang, G. Ye, Internal curing of alkali-activated slag-fly ash paste with superabsorbent polymers, Construct. Build. Mater. 263 (2020) 120985, https://doi.org/10.1016/j.conbuildmat.2020.120985.
[30] P. Lura, M. Wyrzykowski, Influence of Aggregate Restraint on Volume Changes: Experiments and Modelling, Concreep, 2015, pp. 17–23, https://doi.org/10.1061/9780784479346.
[31] R. Naghdi, Evaluation of autogenous shrinkage of high-performance concrete, in: Third Int. Conf. Sustain. Constr. Mater. Technol., 2010. Kyoto.
[32] Y. Wei, W. Hansen, J.J. Biernacki, E. Schlangen, Unified shrinkage model for concrete from autogenous shrinkage test on paste with and without ground-granulated blast-furnace slag, ACI Mater. J. 108 (2011) 13.
[33] G. Pickett, Effect of aggregate on shrinkage of concrete and a hypothesis concerning shrinkage, J. Proc. (1956) 581–590.
[34] D.W. Hobbs, Influence of aggregate restraint on the shrinkage of concrete, ACI J. Proc. 71 (1974) 445–450, https://doi.org/10.14359/7089.
[35] E. Tazawa, R. Sato, E. Sakai, S. Miyazawa, Work of JCI committee on autogenous shrinkage, Shrinkage Concr. Shrinkage (2000) 21–33.
[36] I. Maruyama, A. Sugie, Numerical study on drying shrinkage of concrete affected by aggregate size, J. Adv. Concr. Technol. 12 (2014) 279–288, https://doi.org/10.3151/jact.12.279.
[37] M. Abdellatef, M. Alnaggar, G. Boumakis, G. Cusatis, G. Di-Luzio, R. Wendner, Lattice discrete particle modeling for coupled concrete creep and shrinkage using the solidification microprestress theory, CONCREEP 10 (2015) 184–193.
[38] C. Videla, D.J. Carreira, N. Garner, others, Guide for modeling and calculating shrinkage and creep in hardened concrete, ACI Rep 209 (2008).
[39] H. Zhang, B. Šavija, S.C. Figueiredo, M. Lukovic, E. Schlangen, Microscale testing and modelling of cement paste as basis for multi-scale modelling, Materials (Basel) 9 (2016), https://doi.org/10.3390/ma9110907.

[40] N. Lahmar, F. Bouziadi, B. Boulekbache, E.-H. Meziane, M. Hamrat, A. Haddi, C. Djelal, Experimental and finite element analysis of shrinkage of concrete made with recycled coarse aggregates subjected to thermal loading, Construct. Build. Mater. 247 (2020) 118564.
[41] E. Schlangen, E.J. Garboczi, Fracture simulations of concrete using lattice models: computational aspects, Eng. Fract. Mech. 57 (1997) 319–332.
[42] G. Fang, M. Zhang, Multiscale micromechanical analysis of alkali-activated fly ash-slag paste, Cement Concr. Res. 135 (2020) 106141, https://doi.org/10.1016/j.cemconres.2020.106141.
[43] T. Lu, Autogenous Shrinkage of Early Age Cement Paste and Mortar, Delft University of Technology, 2019.
[44] M. Nedeljković, Carbonation mechanism of alkali-activated fly ash and slag materials. View of Long-Term Performance Predictions, Delft University of Technology, 2019.
[45] M. Nedeljković, K. Arbi, Y. Zuo, G. Ye, Microstructural and mineralogical analysis of alkali activated fly ash- slag pastes, in: Microdurability 2016 Int. Rilem Conf. Microstruct. Relat. Durab. Cem. Compos., 2016.
[46] S.J. Lokhorst, Deformational Behaviour of Concrete Influenced by Hydration Related Changes of the Microstructure, Delft University of Technology, 2001.
[47] Z. Li, S. Zhang, X. Liang, G. Ye, Cracking potential of alkali-activated slag and fly ash concrete subjected to restrained autogenous shrinkage, Cement Concr. Compos. 114 (2020) 103767, https://doi.org/10.1016/j.cemconcomp.2020.103767.
[48] P. Lura, K. Van Breugel, I. Maruyama, Effect of curing temperature and type of cement on early-age shrinkage of high-performance concrete, Cement Concr. Res. 31 (2001) 1867–1872, https://doi.org/10.1016/S0008-8846(01)00601-9.
[49] M.H. Zhang, C.T. Tam, M.P. Leow, Effect of water-to-cementitious materials ratio and silica fume on the autogenous shrinkage of concrete, Cement Concr. Res. 33 (2003) 1687–1694, https://doi.org/10.1016/S0008-8846(03)00149-2.
[50] S. Hanjitsuwan, B. Injorhor, T. Phoo-ngernkham, N. Damrongwiriyanupap, L.Y. Li, P. Sukontasukkul, P. Chindaprasirt, Drying shrinkage, strength and microstructure of alkali-activated high-calcium fly ash using FGD-gypsum and dolomite as expansive additive, Cement Concr. Compos. 114 (2020) 103760, https://doi.org/10.1016/j.cemconcomp.2020.103760.
[51] NEN-EN 12390-3, Testing Hardened Concrete - Part 3: Compressive Strength of Test Specimens, 2009.
[52] A. Fernández-Jiménez, J.G. Palomo, F. Puertas, Alkali-activated slag mortars: mechanical strength behaviour, Cement Concr. Res. 29 (1999) 1313–1321.
[53] F. Puertas, S. Martínez-Ramírez, S. Alonso, T. Vázquez, Alkali-activated fly ash/slag cements. Strength behaviour and hydration products, Cement Concr. Res. 30 (2000) 1625–1632, https://doi.org/10.1016/S0008-8846(00)00298-2.
[54] A.M. Neville, Properties of Concrete, 2011.
[55] ASTM C1968, Standard Test Method for Autogenous Strain of Cement Paste and Mortar, 2013, pp. 1–8, https://doi.org/10.1520/C1698-09.2.
[56] ASTM C191-18a, Standard Test Methods for Time of Setting of Hydraulic Cement by Vicat Needle, 2019, pp. 1–8, https://doi.org/10.1520/C0191-18A.2.
[57] S. Uppalapati, S. Joseph, Ö. Cizer, Autogenous shrinkage and strength development of alkali-activated slag/fly ash mortar blends, in: 5th Int. Slag Valoris. Symp., 2017, pp. 393–396.
[58] Z. Li, M. Nedeljkovic, Y. Zuo, G. Ye, Autogenous shrinkage of alkali-activated slag-fly ash pastes, in: 5th Int. Slag Valoris. Symp., 2017, pp. 369–372. Leuven.
[59] E. ichi Tazawa, S. Miyazawa, T. Kasai, Chemical shrinkage and autogenous shrinkage of hydrating cement paste, Cement Concr. Res. 25 (1995) 288–292, https://doi.org/10.1016/0008-8846(95)00011-9.
[60] E. ichi Tazawa, S. Miyazawa, Influence of cement and admixture on autogenous shrinkage of cement paste, Cement Concr. Res. 25 (1995) 281–287, https://doi.org/10.1016/0008-8846(95)00010-0.
[61] NEN-EN 196-3 + A1, Methods of Testing Cement - Part 3: Determination of Setting Times and Soundness, 2016.
[62] S. Zhang, Z. Li, B. Ghiassi, S. Yin, G. Ye, Fracture properties and microstructure formation of hardened alkali-activated slag/fly ash paste, Cement Concr. Res. (2020) (In revision).
[63] T. Phoo-Ngernkham, C. Phiangphimai, N. Damrongwiriyanupap, S. Hanjitsuwan, J. Thumrongvut, P. Chindaprasirt, A mix design procedure for alkali-activated high-calcium fly ash concrete cured at ambient temperature, Ann. Mater. Sci. Eng. 2018 (2018), https://doi.org/10.1155/2018/2460403.
[64] D. Ravikumar, N. Neithalath, Reaction kinetics in sodium silicate powder and liquid activated slag binders evaluated using isothermal calorimetry, Thermochim. Acta 546 (2012) 32–43, https://doi.org/10.1016/j.tca.2012.07.010.
[65] S. Chithiraputhiran, N. Neithalath, Isothermal reaction kinetics and temperature dependence of alkali activation of slag, fly ash and their blends, Construct. Build. Mater. 45 (2013) 233–242, https://doi.org/10.1016/J.CONBUILDMAT.2013.03.061.
[66] S. Zhang, Y. Zuo, Z. Li, G. Ye, Isothermal calorimetric study on heat evolution and apparent activation energy of alkali-activated slag/fly ash paste. 2nd Int. Conf. Sustain. Build. Mater., 2019, pp. 1–8. Eindhoven.
[67] K.A. Riding, J.L. Poole, K.J. Folliard, M.C.G. Juenger, A.K. Schindler, Modeling hydration of cementitious systems, ACI Mater. J. 109 (2012) 225–234.
[68] L. Taerwe, S. Matthys, Others, Fib Model Code for Concrete Structures 2010, Ernst & Sohn, Wiley, 2013.
[69] British Standards Institution, Eurocode 2: Design of Concrete Structures: Part 1-1: General Rules and Rules for Buildings, British Standards Institution, 2004.
[70] S. Prinsse, D.A. Hordijk, G. Ye, P. Lagendijk, M. Luković, Time-dependent material properties and reinforced beams behavior of two alkali-activated types of concrete, Struct. Concr. 21 (2020) 642–658, https://doi.org/10.1002/suco.201900235.
[71] S.P. Timoshenko, J.N. Goodier, Theory of elasticity (1951) 359.
[72] R.M. Jones, Deformation Theory of Plasticity, Bull Ridge Corporation, 2009.
[73] T.C. Hansen, K.E.C. Nielsen, Influence of aggregate properties on concrete shrinkage, J. Proc. (1965) 783–794.
[74] L.F. Nielsen, A Research Note on Sorption, Pore Size Distribution, and Shrinkage of Porous Materials, Danmarks Tekniske Højskole, Laboratoriet for Bygningsmaterialer, 1991.
[75] T.Y. Zhu, Some useful numbers on the engineering properties of materials (geologic and otherwise), Geol. 615 (2012). Department of Geophysics.
[76] P. Lura, G. Ye, K. van Breugel, Effect of cement type on autogenous deformation of cement-based materials, Spec. Publ. 220 (2004) 57–68.
[77] K. Van Breugel, Relaxation of Young Concrete, 1980, p. 144.
[78] H. van der Ham, E. Koenders, K. van Breugel, Creep model uncertainties in early-age concrete simulations, Proc. Concreep. 8 (2008) 431–436.
[79] L. Lam, Y.L. Wong, C.S. Poon, Degree of hydration and gel/space ratio of high-volume fly ash/cement systems, Cement Concr. Res. 30 (2000) 747–756.
[80] G. Ye, Experimental Study and Numerical Simulation of the Development of the Microstructure and Permeability of Cementitious Materials, 2003.
[81] Y. Zuo, Experimental Study and Numerical Simulation of the Reaction Process and Microstructure Formation of Alkali-Activated Materials, Delft University of Technology, 2019.
[82] A. Darquennes, S. Staquet, M.P. Delplancke-Ogletree, B. Espion, Effect of autogenous deformation on the cracking risk of slag cement concretes, Cement Concr. Compos. 33 (2011) 368–379, https://doi.org/10.1016/j.cemconcomp.2010.12.003.
[83] P. Goltermann, Mechanical predictions on concrete deterioration. Part 1: eigenstresses in concrete, Mater. J. 91 (1995) 543–550.
[84] Y. Wei, Modeling of Autogenous Deformation in Cementitious Materials, Restraining Effect from Aggregate, and Moisture Warping in Slabs on Grade, University of Michigan, 2008.
[85] S. Altoubat, D. Lange, Creep , Shrinkage and Cracking of Restrained Concrete at Early Age, 2001, 0–31.
[86] F. Wittmann, Bestimmung physikalischer Eigenschaften des Zementsteins, 1974.
[87] H. Zhang, B. Šavija, Y. Xu, E. Schlangen, Size effect on splitting strength of hardened cement paste: experimental and numerical study, Cement Concr. Compos. 94 (2018) 264–276.